

Physical Limits of Hyperthermia Using Magnetite Fine Particles

Rudolf Hergt, Wilfried Andrä, Carl G. d'Ambly, Ingrid Hilger, Werner A. Kaiser, Uwe Richter, and Hans-Georg Schmidt

Abstract—Structural and magnetic properties of fine particles of magnetite are investigated with respect to the application for hyperthermia. Magnetic hysteresis losses are measured in dependence on the field amplitude for selected commercial powders and are discussed in terms of grain size and structure of the particles. For ferromagnetic powders as well as for ferrofluids, results of heating experiments within organic gels in a magnetic high frequency field are reported. The heating effect depends strongly on the magnetic properties of the magnetite particles which may vary appreciably for different samples in dependence on the particle size and microstructure. In particular, the transition from ferromagnetic to superparamagnetic behavior causes changes of the loss mechanism, and accordingly, of the heating effect. The maximum attainable heating effect is discussed in terms of common theoretical models. Rise of temperature at the surface of a small heated sample as well as in its immediate neighborhood in the surrounding medium is measured in dependence on time and is compared with solutions of the corresponding heat conductivity problem. Conclusions with respect to clinical applications are given.

Index Terms— Hysteresis, losses, relaxation, superparamagnetism.

I. INTRODUCTION

APPLICATION of magnetic materials for hyperthermia of biological tissue has been known in principle for more than four decades (e.g., [1]). Many empirical work was done in order to manifest a therapeutic effect on several types of tumors by performing experiments with animals (e.g., [2]) or using cancerous cell cultures (e.g., [3]). However, routine medical applications are not known until now, and there is a demand for more profound understanding of the physical limits of that method to render it reliable for tumor therapy of human beings. Magnetic media were applied in several ways using glass ceramics [2], microcapsules [4], or suspensions of magnetic fine particles (e.g., [5]). In order to select an appropriate material, medical compatibility has to be considered. Preferentially, several types of magnetic oxides were used, among which, magnetite is a very promising

candidate since its biocompatibility was already proven. In any case, a large heating power of the material is desirable in order to reduce the amount of material to be applied to the patient. The heating effect, i.e., the spatial distribution and temporal development of temperature in the tumor region, must be precisely predetermined by choosing correct external technical parameters. Therefore, for a reliable dosage, the underlying physics has to be thoroughly understood. The very important biological and medical problems (e.g., targeting of the particles, temperature influence on several tissues or specific cells, combination of heating with other therapeutical means) are beyond the scope of the present paper.

The heating of magnetic oxides with low electrical conductivity in an external alternating magnetic field is mainly due to either loss processes during the reorientation of the magnetization (e.g., [6], [7]) or frictional losses if the particle can rotate in an environment of sufficiently low viscosity [11]. Inductive heating of magnetic oxides (i.e., via eddy currents) may be neglected. The losses due to magnetization reorientation in ferro- or ferrimagnetic particles depend on the type of remagnetization process (wall displacement or several types of rotational processes) which is determined besides by the intrinsic magnetic properties like magnetocrystalline anisotropy and exchange coupling constant—in complicated ways by particle size, shape and microstructure (e.g., [6]–[8]). It is known that magnetic properties of powders may vary significantly in dependence on grain size and particle microstructure. For sufficiently small single domain particles, thermal fluctuations lead to an activation of remagnetization processes since the energy barrier for reorientation of the magnetic moment of the particle decreases with decreasing particle volume. In dependence on temperature and measurement frequency, thermal fluctuation aftereffects may be observed (e.g., [6], [7]). An external alternating magnetic field supplies energy and assists magnetic moments in overcoming the energy barrier. This energy is dissipated when the particle moment relaxes to its equilibrium orientation. The losses caused by this so-called Néel relaxation [9], [10] lead to heating of the particle ensemble and may be used for hyperthermia.

Besides the losses caused by magnetization rotation inside the particles, another loss type may arise in the case of ferrofluids which is related to the rotational Brownian motion of the magnetic particles [11]. In this case, the energy barrier for reorientation of a particle is determined by rotational friction within the suspension fluid of viscosity η . In addition, at high frequency (e.g., GHz range) depending on the anisotropy

Manuscript received April 8, 1997; revised February 11, 1998. This work was supported by the Thüringer Ministerium für Wissenschaft, Forschung und Kultur under Contract B 303-95046.

R. Hergt, W. Andrä, C. G. d'Ambly, and H.-G. Schmidt are with the Institut für Physikalische Hochtechnologie e. V., D-07743 Jena, Germany.

I. Hilger and W. A. Kaiser are with the Institut für Diagnostische und Interventionelle Radiologie of the Friedrich-Schiller-Universität, D-07740 Jena, Germany.

U. Richter is with the Labor für Elektronenmikroskopie, D-06120 Halle/Saale, Germany.

Publisher Item Identifier S 0018-9464(98)04302-7.

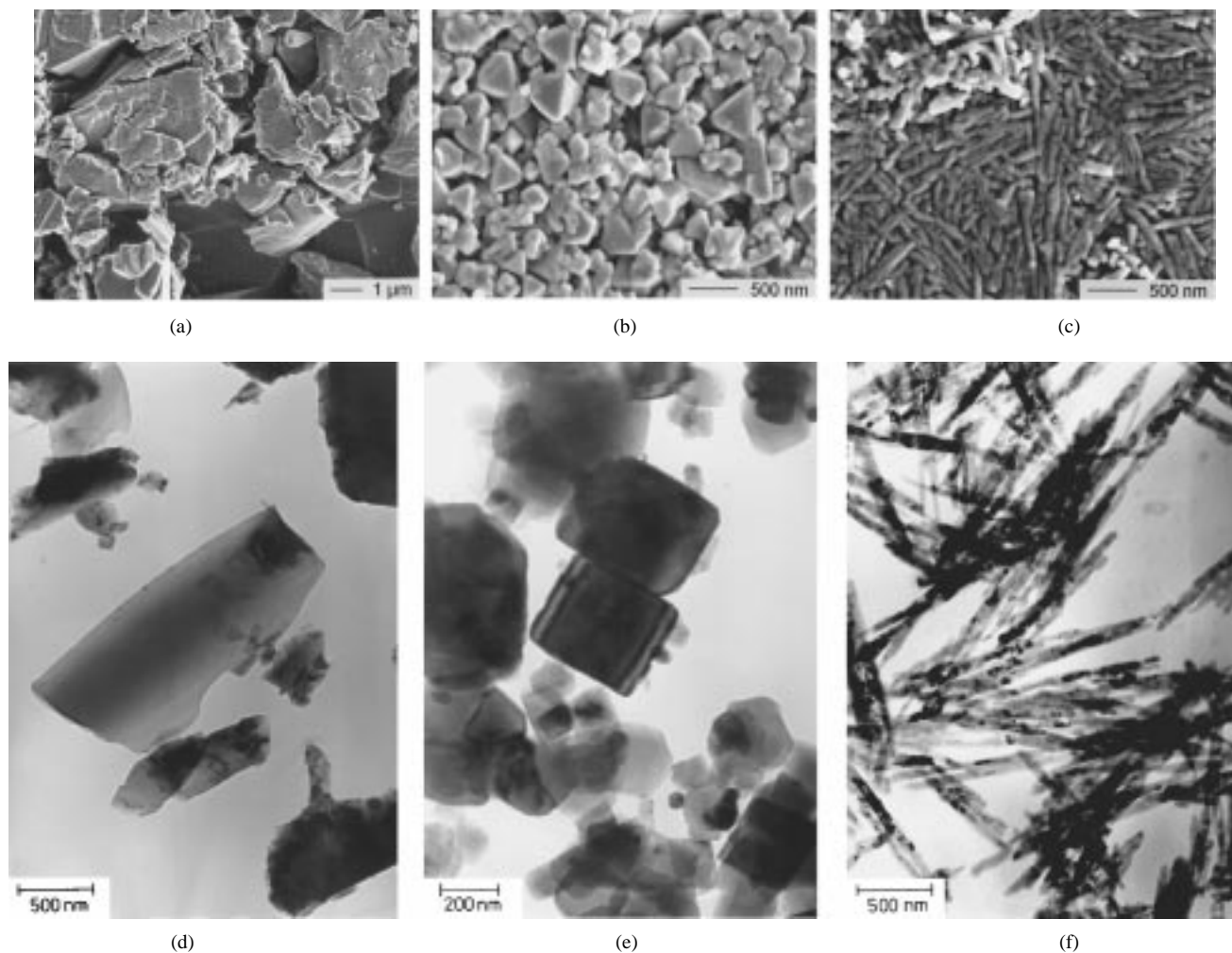


Fig. 1. Structure of the magnetic powders of sample I (a) and (d), sample II (b) and (e) and sample III (c) and (f) investigated by SEM (a), (b), (c) and TEM (d), (e), (f).

field losses related to the ferrimagnetic resonance may occur. Neglecting the last loss type since in the relevant frequency range inductive heating of biological tissue is caused, all other losses are of interest for local magnetic hyperthermia. Microscopically, the energetical barriers involved in the remagnetization process determine the magnetic losses which cause, in dependence on the thermal conductivity and heat capacity of the surrounding medium, a temperature rise of the magnetic material. The specific loss power of the magnetic material should be as high as possible in order to reduce the dose being applied to the patient to a minimum level. Though there are much empirical results on hyperthermia in the literature, there is a lack of more profound understanding of the physical limits of specific loss power, in particular for the transitional region from hysteretic single-domain to superparamagnetic behavior. Accordingly, in the present paper results of a study of the physics of hyperthermia on the base of comparative experimental and theoretical investigations are reported. We compare magnetic properties of selected types of fine magnetite particles of different size and microstructure. The results will be discussed with respect to different contributions of magnetic losses and its physical limitations. Finally, limitations for the spatial distribution and the time dependence

of temperature enhancement in hyperthermia are discussed basing on theoretical and experimental investigations of the heat conduction problem.

II. SAMPLES

Several types of commercially available fine particles of magnetite (Fe_3O_4) were selected in order to investigate the influence of particle properties which are important for the heating effect. These materials were characterized with respect to the size and shape of the particles using scanning electron (SEM) as well as transmission electron microscopy (TEM). Two groups of samples may be differentiated according to the amount of hysteresis losses measured at 50 Hz: type A showing ferromagnetic hysteresis loops (samples I–III) and type B with superparamagnetic behavior, i.e., samples exhibiting almost no losses if measured at 50 Hz (samples IV–VII). From several investigated commercial powders of type A, three typical kinds were selected for the present paper, which are shown in Fig. 1. The particle shape differs remarkably according to the preparation process. For instance, the coarse-grained powder of sample I [Fig. 1(a)] shows clearly features of crushing while at the particles of sample II [Fig. 1(b)] the octahedral habit faces of the spinel structure

TABLE I
PROPERTIES OF MAGNETITE PARTICLES

Samples	SEM d (nm)	TEM d (nm)	X-ray d (nm)	Shape	Loss power p (W/g) ¹⁾
Sample I	> 1000	350	250	crushed	75
Sample II	250	250	200	polyhedra	42
Sample III	60 x 250	50 x 1500	50	needles	3

¹⁾ loss power per mass Fe₃O₄ for a field amplitude of 14 kA/m and 300 kHz frequency

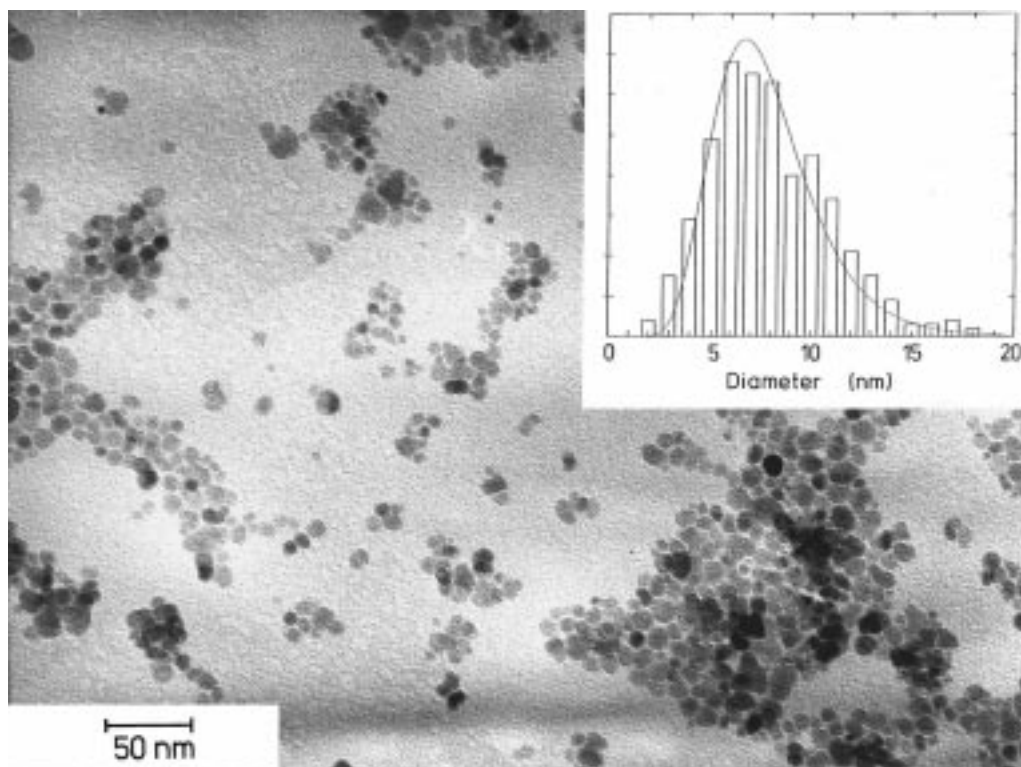


Fig. 2. TEM micrograph of magnetite particles of ferrofluid (sample IV). Inset: size distribution with lognormal fitting curve.

may be recognized which indicate the near equilibrium growth of those particles. Contrarily, particles of sample III [Fig. 1(c)] have an elongated shape being favorably used for magnetic recording media which are prepared according to a special procedure.

In order to get reliable information on the relative broad particle size distributions of the materials shown in Fig. 1, a series of electron-microscopic images was taken by SEM as well as TEM, for comparison. Moreover, line width analysis of X-ray diffraction data was performed using a Philips Xpert diffractometer with the Philips software "Line Profile Analysis." The average size resulting from different characterization methods compared in Table I differ typically due to different ways of preparation of SEM and TEM specimens. Comparison of Fig. 1(a) and (d), for instance, shows that the crushed grains of sample I in the SEM image tend to agglomerate to bigger particles. While SEM gives better information on particle shape especially for coarser materials, the TEM images of individual particles also give, besides particle shape, information on the internal structure (strain, grain boundaries, dislocations). For instance, Fig. 1(f) demonstrates clearly that

each needle shown in Fig. 1(c) consists of many crystallites, a fact which is important for the loss mechanism. In difference to the electron microscopic imaging techniques, X-ray diffraction gives a measure of the coherent scattering volume, i.e., the size of single crystalline domains of the particles. The mean X-ray size is smaller than the values deduced from imaging techniques because particles obviously are not completely single crystalline but contain grain boundaries. This is also confirmed by TEM, in particular in the case of the crushed and the fibrous material of samples I and III, respectively. Size distributions are lognormal with standard deviations in the order of two times the average. All images of Fig. 1 as well as data of Table I refer to uncoated particles.

All samples just discussed show ferromagnetic behavior i.e., considerable hysteresis at 50 Hz. With decreasing particle size, one observes in dependence on the characteristic time of measurement, a transition to superparamagnetic behavior, i.e., vanishing of hysteresis. For comparison, we have investigated some typical samples of commercially available ferrofluids consisting of fine particles of magnetite. Fig. 2 shows a TEM micrograph of sample IV which is representative for ferrofluid

TABLE II
PROPERTIES OF FERROFLUIDS

Samples	Mean grain diameter d (nm)	Suspension	Loss power p (W/g) ¹⁾	Loss power p (W/g) ²⁾
Sample IV	10	kerosene	45	209
Sample V	10	esther	29	135
Sample VI	8	aequous	21	97
Sample VII	6	aequous	< 0.1	< 0.5

¹⁾ loss power per mass Fe_3O_4 measured at 300 kHz and 6.5 kA/m field amplitude

²⁾ calculated for 14 kA/m assuming square dependence of loss power on the field amplitude

samples V and VI, too. The size distribution shown as inset of Fig. 2 may be well fitted with a lognormal law. In Table II, mean grain sizes of ferrofluid samples are given together with suspension base as well as loss power data measured at 300 kHz which will be discussed below. The given average size refers to the magnetite core. Size distributions are lognormal with standard deviation in the order of half of the average. In particular, with sample VII we have tested the applicability for hyperthermia of the approved pharmaceutical ENDOREM® (Guerbet) which is used as a contrast medium for magnetic resonance imaging. The mean size of the magnetite particles of that material is only about 6 nm diameter as determined from the magnetization curve measured with a vibrating sample magnetometer. It should be pointed out that samples IV–VII are liquid suspensions. The loss power may depend on the viscosity of the suspension medium as will be discussed below. The effect of different coatings as well as dispersants was not investigated since it is beyond the aim of the present paper. A contribution to that problem may be found in [3].

III. MAGNETIC LOSSES

A. Magnetic Hysteresis Loops

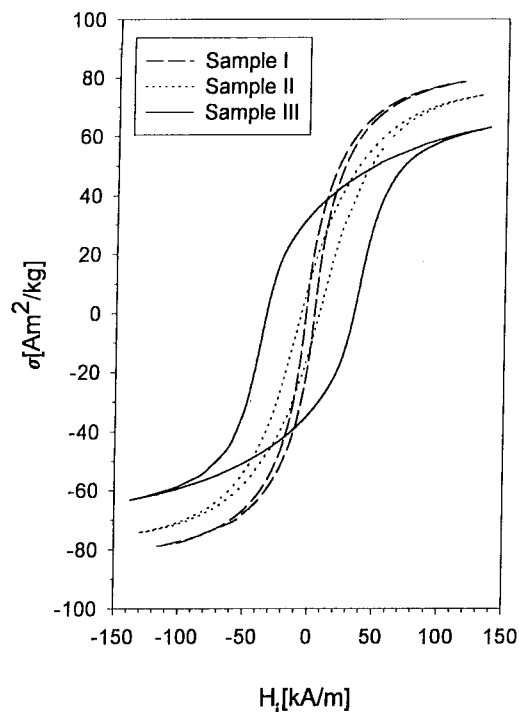
Hysteresis loops of different samples were measured using a hysteresemeter M2000 (Systemes Informatiques, Industrielles et Scientifiques, Buc) at a measuring frequency of 50 Hz. As typical examples, loops of sample I–III are shown in Fig. 3(a). The comparison of these loops demonstrates the great differences which may occur for different magnetite powders due to the influence of particle size, shape, and microstructure. The narrow loops of samples I and II with a rather high initial permeability and low coercivity of 3.3 and 7.5 kA/m, respectively, indicate that remagnetization in these particles occurs via domain wall displacement. According to the mean grain diameter d given in Table I, the typical multidomain particle behavior is found which is theoretically predicted for nearly cubic grains above a size of 100 nm [12]. The measured coercivity values are in agreement with data given by Heider *et al.* [8]. These authors have shown that for most empirical data of magnetite the size dependence of coercivity H_c and remanence M_r follows a power law of about $d^{-0.6}$. From grain images one may estimate that the shape anisotropy of particles from samples I and II is not much larger than the rather low value of the cubic magnetocrystalline anisotropy of magnetite. Contrarily, sample III shows the

typical hard magnetic behavior of elongated particles being usually applied for magnetic recording media. Obviously, the extreme aspect ratio of the particles of ten which may be extracted from the TEM images is the reason for a large shape anisotropy which represents the barrier for particle remagnetization. This sample dominated by single domain behavior (rotational processes, buckling, or curling [6], [7]) exhibits large coercivity of 34 kA/m and very high hysteresis losses. At first sight, this material seems to be very suitable for magnetic heating. However, in hyperthermia, rarely the full hysteresis loop of such samples can be used since there are restrictions of the field amplitude mainly for technical reasons. Consequently, for single domain particle ensembles with a nearly rectangular hysteresis loop, one may expect a rapid decrease of losses for field amplitudes below the effective anisotropy field. As an example, in Fig. 3(b) a series of minor loops of sample III is given which shows that the loop area is rapidly reduced with decreasing field amplitudes.

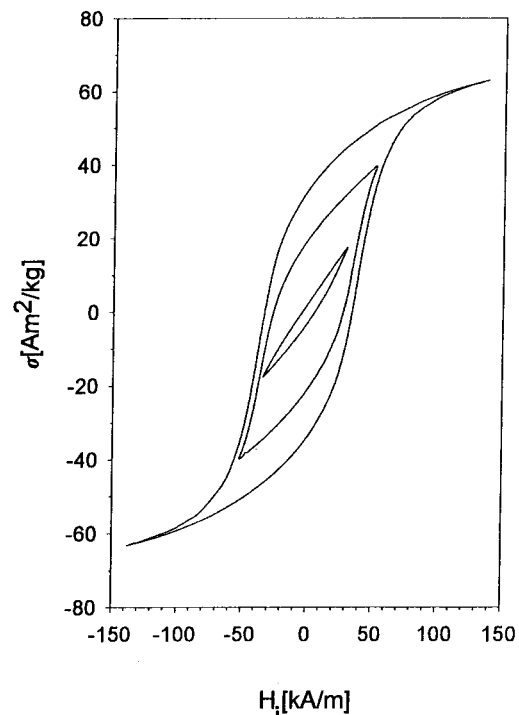
With decreasing particle size the energetic barriers involved in the remagnetization process decrease and relaxation effects (creep) may occur. A narrowing of hysteresis loops is observed if the characteristic time of measurement is much longer than the relaxation time. For samples IV–VII we see accordingly no opening of the hysteresis loop at 50 Hz within the scale of Fig. 3(a). Coercivities are below 1 kA/m. However, it has to be pointed out that the transition to superparamagnetism occurs in a very narrow frequency range depending on mean particle size (see below), i.e., particles which show so-called superparamagnetic behavior in loop measurements at 50 Hz may give full hysteresis losses at 500 kHz.

B. Hysteresis Losses

In general, magnetic losses of different materials may show very different nonlinear dependence on the field amplitude. In the literature, field dependence for small amplitudes often is described by a square law (e.g., [3], [5]) which however is a rather rough approximation. Hysteresis losses for so-called Rayleigh loops (e.g., [6], [7]) may be well described by a third order power law. In order to evaluate the maximum power to be deposited in cancerous tissue by means of hysteresis losses, we have determined the dependence of hysteresis losses on the field amplitude by integrating the loop area of measured minor loops. Results are shown for samples I–III in Fig. 4. Near 35 kA/m there is a crossover of the curves above which the rank order of the three samples with respect to their



(a)



(b)

Fig. 3. (a) Saturation hysteresis loops of samples I–III measured at 50 Hz. H_i is the internal field deduced from the applied field by taking into account the demagnetization effect. (b) Hysteresis loops of sample III for three different loop amplitudes measured at 50 Hz.

specific loss power is reversed. Obviously, in the case of sample III, by low field amplitudes one rarely may change the magnetization direction of the single domain particles with high shape anisotropy. Unfortunately, there are considerable problems with the application of high amplitude magnetic ac-

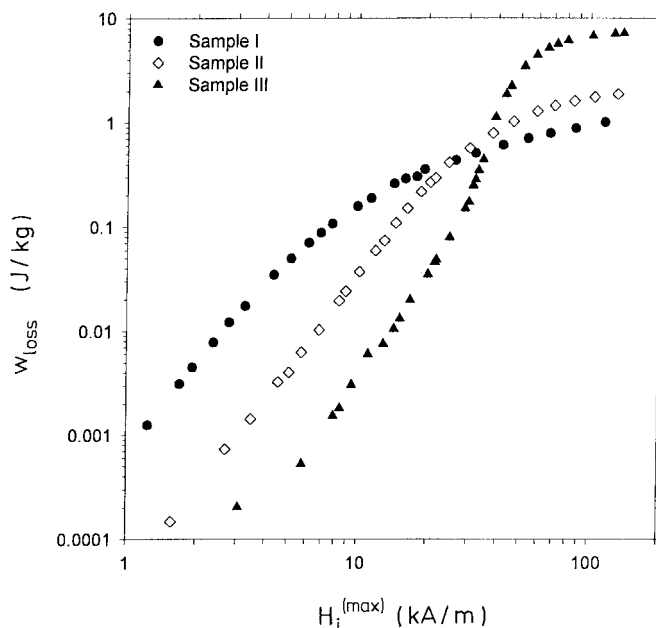


Fig. 4. Magnetic hysteresis losses in dependence on the magnetic field amplitude $H_i^{(\max)}$ for 50 Hz.

fields to a human patient. Therefore, losses being useful for hyperthermia are very low for material III which is superior to all other ones if driven to saturation. Contrary, in sample I which consists at least partially of multidomain particles, one may assume that the mechanical work that the sample has undergone during preparation resulted in domain wall pinning centers which cause relatively high losses already at low field amplitudes.

From measured hysteresis loss one may easily estimate the power deposited in an alternating field by taking into account the proportionality of power with frequency. Values of hysteresis loss power estimated in this way agree well with results of calorimetric determination of the heat power deposited in a medium of known heat capacity as described in Section IV-B. Values of loss power of samples I–III determined in this way for a high frequency field with typical parameters of 14 kA/m amplitude and 300 kHz frequency are compiled in Table I.

The upper physical limit of power density attainable by means of hysteresis losses is given in the case of a nearly rectangular hysteresis loop by $4\mu_0 M_s H_s (H_s = 2K/(\mu_0 M_s))$, M_s saturation magnetization, K anisotropy energy density). However, this loop type is found only for an ensemble of aligned uniaxial particles with the external ac-field parallel to the easy axis. This case hardly will be realizable in hyperthermia application. For the case of statistically oriented particles one has approximately the relative remanence $M_r/M_s = 0.5$ and coercivity $H_c = 0.5H_s$. Hysteresis loss is reduced by about a factor of 0.25 in comparison to the aligned case (for details see e.g., [6]). According to the empirically well established size dependence of coercivity H_c and remanence M_r , referred in Section III-A, above the critical grain size (see below) there is a power law increase of losses with decreasing particle size. Taking experimental data given in [8] for precipitated magnetite grains one may estimate for instance for a particle

diameter of 50 nm an upper limit of about 1.5 J/kg which gives for a frequency of 300 kHz a loss power of 450 W/g. For crushed material, even higher values should be possible. In comparison, the experimentally found losses given in Table I are much smaller mainly due to larger grains and because limitations of the field amplitude discussed above do not allow utilization of the complete hysteresis loop. For instance, for sample III which at 300 kHz gave only 3 W/g for reasonable field amplitude of 14 kA/m, one may estimate from the experimental data of Fig. 4 a loss power of 2.4 kW/g for the full hysteresis loop (100 kA/m).

With decreasing particle size the probability of spontaneous magnetization jumps due to thermal activation increases, and relaxational effects may be observed in dependence on the measurement frequency ω . The measurement frequency defines the so-called critical grain volume V_c for which $\omega\tau = 1$ (τ magnetic relaxation time discussed below). Near this critical size, relaxation effects cause a rapid decrease of the remanent magnetization

$$M_r = M_{r0} \exp(-t/\tau) \quad (1)$$

(M_{r0} remanence for particles unaffected by relaxation). At the same time the coercivity decreases rapidly with decreasing particle size which may be described by [6]

$$H_c = (2K/M_s) \left[1 - (V_c/V)^{1/2} \right], V > V_c. \quad (2)$$

Consequently, hysteresis losses vanish abruptly near the critical particle size. For a measuring frequency of 300 kHz and a magnetocrystalline anisotropy energy density of 10^4 J/m³ (due to e.g., ellipsoidal shape with an aspect ratio of 1.4) critical size is about 20 nm diameter.

C. Relaxational Losses

For samples IV–VII which show negligible hysteresis losses at 50 Hz, loss power was measured calorimetrically at 300 kHz as described below. The results given in Table II as well as data reported in the literature [3], [5] show that also with “superparamagnetic” particle ensembles considerable heating effects may be observed. However, comparing samples VI and VII for instance shows that the results may deviate extremely for apparently similar samples. We will discuss these results in comparison to theoretical estimations of relaxational losses.

Losses arising in the superparamagnetic grain size region may be well understood for the simple model case that there are only two metastable antiparallel orientations of the particle magnetic moment m . The corresponding two energy levels are separated by an energy barrier given by the anisotropy energy KV (V particle volume). Assuming a rather high energy barrier $KV \gg kT$, the relaxation time of the system is determined by the ratio of anisotropy energy KV to thermal energy kT [6], [7], [9], [10]

$$\tau = \tau_o \exp[KV/(kT)] \quad (3)$$

($\tau_o \sim 10^{-9}$ s).

The time evolution of the system may be described using a master equation approach for the occupation numbers n_+ and n_- in the two states (e.g., [13]–[15]). The difference of

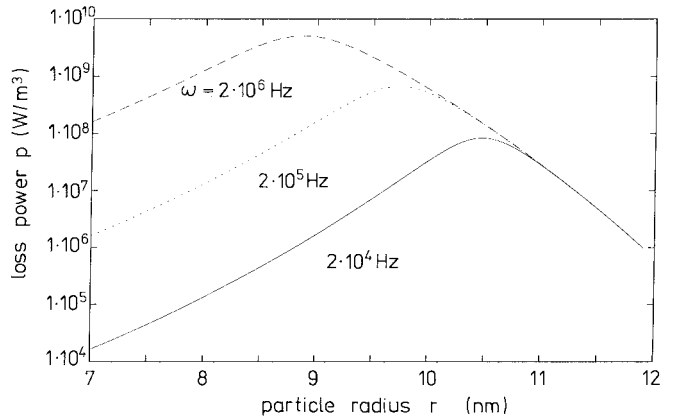


Fig. 5. Grain size dependence of the loss power density due to Néel-relaxation for small ellipsoidal particles of magnetite (field amplitude 6.5 kA/m).

the occupation numbers Δn gives the magnetization of the particle system $M = m\Delta n$ (m is the particle moment). The transition probabilities in the presence of an external magnetic field H are given by

$$w_{\pm} = (1/2\tau) \exp[\pm mH/(kT)]. \quad (4)$$

For small fields $mH \ll kT$, the exponential may be replaced by a first order approximation and the rate equation gives for an alternating external field $H_0 \exp(i\omega t)$ of frequency ω and amplitude H_0 the time dependence of the magnetization [14]

$$M(t) = (nm^2/kT)(1 + i\omega\tau)^{-1} H_0 \exp(i\omega t) \quad (5a)$$

$$(n = n_+ + n_-).$$

Hence, in this way, the complex susceptibility for small field amplitudes is known and one may determine from the imaginary part the specific loss power P as usual (e.g., [16])

$$P = (mH\omega\tau)^2 / [2\tau kTV(1 + \omega^2\tau^2)]. \quad (5b)$$

According to this equation, at low frequencies ($\omega\tau \ll 1$), i.e., approaching the superparamagnetic regime, losses increase with the square of frequency while for $\omega\tau \gg 1$ relaxational losses saturate at $P = (mH)^2 / (2kTV\tau)$, i.e., losses are independent on frequency. The transition between these two regimes takes place near $\omega\tau = 1$. There, the imaginary part of the magnetic susceptibility has its maximum and accordingly the dependence of losses on grain size shows a sharp maximum. Note that the relaxation time τ in (5b) depends strongly on the particle size according to (3). Fig. 5 shows the particle size dependence of the loss power density due to Néel relaxation calculated according to (5b) for three values of the measuring frequency ω . Parameters were chosen according to the goal of application for hyperthermia. The frequency $f = 300$ kHz ($\omega = 2 \times 10^6$ s⁻¹) together with a field amplitude of 6.5 kA/m is at the higher end of what may be applied to a tumor patient. The actual value depends strongly on the particular situation: the position of the carcinoma, the case history of the patient, and until now, not completely clear criteria of magnetic field tolerance for tumor patients. Materials parameters were taken for small magnetite ellipsoids: $M_s = 4.7 \times 10^5$ A/m, $K = 10^4$ J/m³ (shape

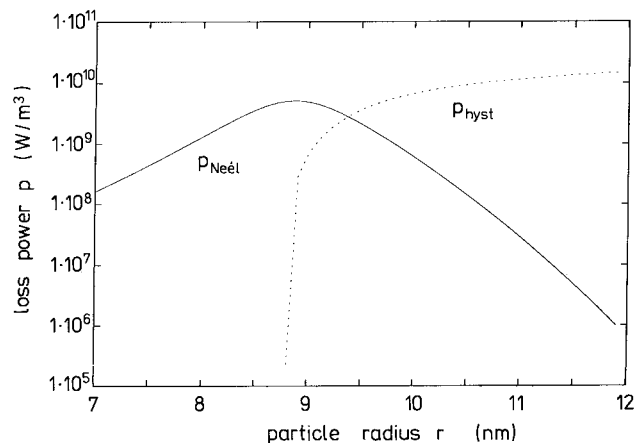


Fig. 6. Dependence of magnetic loss power density on particle size for magnetite fine particles (dotted line—hysteresis losses, full line—Néel losses; frequency $2 \times 10^6 \text{ s}^{-1}$, field amplitude 6.5 kA/m).

anisotropy due to an aspect ratio of 1.4). There is a very sharp maximum of loss power versus particle size. This strong size dependence may be one of the reasons for the abrupt decline of loss power with decreasing particle size comparing samples VI and VII in Table II. However, one has to note that those samples have size distributions which partly overlap and other reasons may additionally contribute to the found differences.

In order to go a step further to understand loss power limitations of fine magnetite particles let us now compare the size dependence of Néel losses with that of hysteresis losses. From the discussion of the latter one in Section III-B we know that hysteresis losses increase with decreasing grain size until they abruptly decline near the critical grain volume V_c . Fig. 6 shows this decline in the critical grain size region for spherical particles using equations given in Section III-B. Calculations were done for magnetic parameters of magnetite assuming $M_{ro} = 0.5M_s$. In addition, the contribution of Néel losses for particles with radius near the critical size are shown according to (5b) where the above given magnetite parameters, field amplitude $H = 6.5 \text{ kA/m}$, and frequency $\omega = 2 \times 10^6 \text{ s}^{-1}$ are assumed. Note that the critical particle size for which remanence and coercivity vanish depends on the measurement frequency. For instance, for common observation times corresponding to magnetization measurements using a vibrating sample magnetometer, the critical size is in the order of 40 nm particle diameter. At higher frequencies applied for hyperthermia, the critical size defined by $\omega\tau = 1$ is considerably smaller. It is shown in Fig. 6 that in the critical particle size region where hysteresis losses vanish, Néel losses grow as a new loss mechanism which, roughly speaking, extends the loss region toward even smaller particle sizes.

Of course the range of validity of the theoretical model assumptions have to be kept in mind when compared with experimental results. First, the condition of large energy barrier ($KV \gg kT$) may be violated for very small particle size. In this case the simple exponential dependence of the relaxation time on the energy barrier used in (3) is a too rough approximation so that more sophisticated methods for the calculation are necessary (e.g., [15]). Secondly, deviations may occur for large field amplitudes i.e., when the condition $mH \ll kT$ is

not fulfilled. In this case the linear response theory may be insufficient and the consideration of nonlinear susceptibility effects is necessary. In our case a particle diameter smaller than about 20 nm is demanded which is usually met for ferrofluids. Further, the above given estimations have to be modified by taking into account size distributions as well as distributions of magnetic parameters, in particular, anisotropy fields (cf. e.g., [13]).

In principle, in ferrofluids besides the just discussed main loss contributions, relaxation may also occur due to rotational Brownian motion of the magnetic particles [11]. This effect becomes essential if the magnetic moment direction is strongly coupled to the particle itself, e.g., by a large value of the intrinsic magnetic anisotropy, combined with easy particle reorientation due to a low viscosity η of the suspension medium. For spherical particles with the hydrodynamical radius r_h (which due to, e.g., a particle coating usually is larger than the magnetic particle radius) the relaxation time is given by [7]

$$\tau_B = 8\pi\eta r_h^3 / (kT). \quad (6)$$

The loss power is approximately given by (5b) taking (6) as relaxation time. In a general case when both Néel and Brown relaxation mechanisms are present, the effective relaxation time may be estimated as $\tau_{\text{eff}} = \tau_N \tau_B / (\tau_N + \tau_B)$. However, regarding relevant viscosity data, Brownian relaxation may be considered as ineffective in biological tissue.

There may exist an additional relaxation process when the magnetic moment may change its orientation continuously which is not taken into account by the simple two-state model. This is the case for relaxation inside of a potential minimum for the magnetization orientation which is well known in ferromagnetic resonance (FMR) where it determines the width of the FMR line. In principle, this relaxation mechanism should also exist in the large dissipation limit, but the possible contribution to hyperthermia is not clear up to now.

Besides the above discussed particle parameters: size, remanence, and coercivity (which strongly depend on the grains microstructure) there are other parameters which influence magnetic losses. The strong effect of the shape was demonstrated by the discussion of the properties of sample III. Moreover, an essential influence of particle coating in colloidal magnetite was reported which however is beyond the scope of the present paper. Chan *et al.* [3] have reported for dextran-stabilized ferrocolloids remarkable effects of proper preparation procedures (e.g., ultrasonic treatment) on power density.

IV. TEMPERATURE ENHANCEMENT

The ultimate goal of hyperthermia for therapy of cancer is to generate a well defined temperature field at the tumor. Providing the problem of depositing the magnetic heating agent at the locus of interest has been solved, however, there remain questions of the time regime and the spatial distribution of temperature, especially the maximum temperature attainable by a defined amount of applied power. There, the distribution of magnetic particles in the tissue and the heat depletion due

to conduction in the tissue as well as due to transportation by flowing blood is essential. In particular, the latter contribution to heat depletion is temperature dependent due to vasodilatation with increasing temperature. To a certain extent, one may take into account the effect of blood perfusion by using some effective heat conductivity. However, the influence of larger blood vessels ought to be investigated in more detail (see e.g., [17]). As a first approximation we have solved the problem of heat depletion for the simplified case of a power absorbing sphere embedded in a homogeneous medium of finite heat conductivity and compare the results with model heating experiments.

A. Theoretical Estimations

Assume the heat source of power density P is concentrated within a small spherical volume (radius R) surrounded by a medium of homogeneous heat conductivity. The heating material and the surrounding medium are characterized by their values of heat conductivity λ , specific heat capacity c , and mass density ρ . In that case of spherical symmetry and a homogeneous time-independent power density P inside the sphere, the equilibrium temperature (i.e., for a large heating time $t \rightarrow \infty$) as a function of the distance r from the center and counted from the starting temperature before heating is given by [18]

$$\Delta T = P \cdot [R^2 - r^2 + 2R^2\lambda_1/\lambda_2]/(6\lambda_1), \quad (r < R) \quad (7a)$$

$$\Delta T = PR^3/(3\lambda_2 r), \quad (r > R) \quad (7b)$$

neglecting a contact-heat resistance at $r = R$. The index i corresponds to the material inside ($i = 1$) and outside ($i = 2$) of the sphere. The equilibrium distribution given by (7) is plotted in reduced units in Fig. 7(a).

With respect to clinical applications, the rise of temperature as a function of time must be known in order to choose the appropriate time regime. In this case, the solution of the problem is more complicated. Fig. 7(b) shows results of numerical calculations carried out. Here, the values of λ_2 , ρ_2 , and c_2 are taken for water which is not very different from biological tissue in this respect. Furthermore, $\lambda_2/\lambda_1 = 0.5$, $R = 2.3$ mm, and $P = 13.7$ W/cm³ were taken as typical values being representative for our experimental conditions. Fig. 7(b) clearly shows the effect of heat conduction outside the sphere resulting not only in a rather steep temperature gradient near the sphere surface but also increasing with the distance in a delay of the time at which 90% of the respective equilibrium temperature is reached. This delay ranges from 12 min at the surface to about 20 min at a distance $r = 3R$. Delay-times of this order of magnitude have been experimentally observed by Sato *et al.* [4] with *in situ* heating of dog kidneys.

B. Experimental

In order to experimentally test the theoretical solution of the heat conductivity problem we have chosen in a first simulation experiment a very defined heating source avoiding any disturbing effects on the temperature sensors due to high frequency fields. A small resistor with a volume of about 0.05

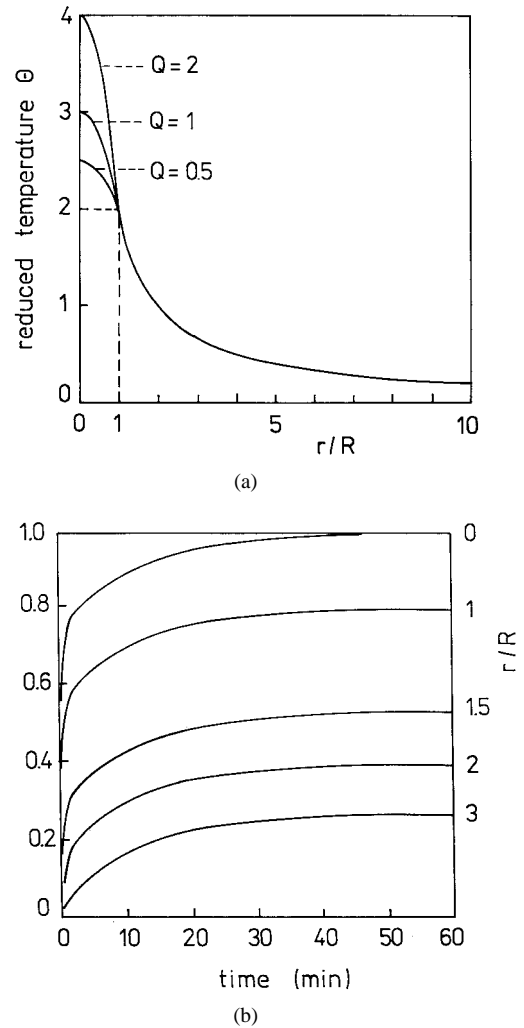


Fig. 7. (a) Spatial distribution of the equilibrium temperature in reduced units. The reduced temperature is defined as $\Theta = 6\Delta T\lambda_2/(PR^2)$ where ΔT means the temperature increase, λ_2 is the heat conductivity outside of the sphere (radius R), and P is the power density. $Q = \lambda_2/\lambda_1$ is the ratio of the heat conductivities outside and inside of the sphere. (b) Calculated temperature increase caused by a heated sphere (radius $R = 2.3$ mm) at different distances r from its center for a power density of $P = 13.7$ W/cm³. $\Delta T_m = 36.4$ K is the temperature increase in the center of the sphere for infinite time.

cm³ was embedded in a large volume of KCl/Carrageenan-gel and was electrically heated by 50 Hz ac-current. The temperature was measured by Cu-Constantan thermocouples placed at different distances from the heating source. Because of its nonspherical shape, the resistor was approximated by a sphere of the same volume having a radius $R = 2.3$ mm. Fig. 8 shows the temperature increase during about 10 min heating measured at different distances from the heating source. A realistic comparison with the above given theoretical results is reasonable, since the parameters used in Fig. 7(b) correspond to those of the experiment. The values of heat conductivity and heat capacity of the resistor were approached by taking 1.6 W/m \times K and 0.4 J/g \times K, respectively. Both experimental and theoretical curves demonstrate, first, the temporal delay of temperature rise and, second, the expected decrease of temperature with the distance from the heating source. That means considering the narrow temperature tolerances in medical applications of local hyperthermia, the heat distribution into

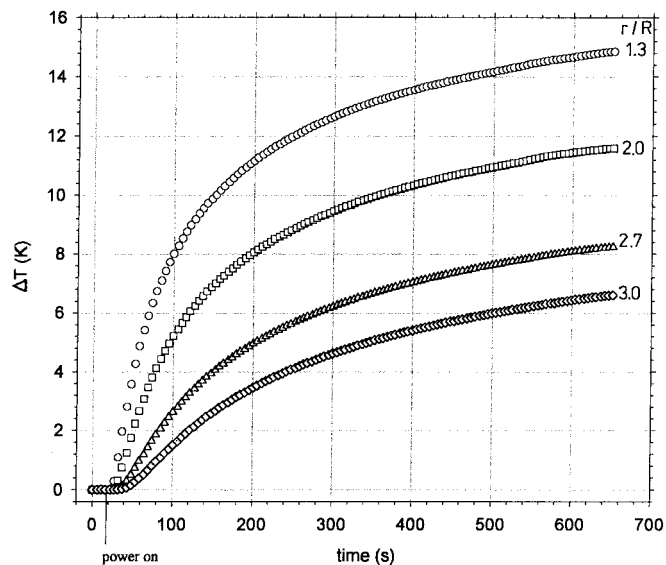


Fig. 8. Temperature increase ΔT at different positions r within a gel heated locally at $r = 0$ by an electrical power of 0.7 W using a small resistor (volume 0.05 cm³).

the environmental tissue must be carefully taken into account for tumor therapy.

Heating experiments for comparing the heating capability of different types of magnetite particles were performed in a simple arrangement using a water cooled coil of 9 cm diameter consisting of three turns. The ac field is generated by means of a commercial generator HFP 061/05 (EFD Induktionserwärmung Fritz Düsseldorf GmbH) with a power of 5 kW. Particles to be investigated were homogeneously dispersed in a relatively large volume of KCl/Carrageenan-gel which was kept in a thermally isolated glass container inside the ac field coil. The dissipated power due to the applied magnetic ac field was determined by measuring the initial slope of the temperature rise by means of a thermocouple immersed into the center of the gel body. Data for the investigated samples are compiled in Tables I and II. For comparison, the loss power was determined from measured hysteresis losses assuming a linear frequency dependence. There is at least for non-relaxing particles good agreement with the calorimetrically determined loss power. By measurement at two frequencies (300 and 4 MHz) the expected proportionality of loss power with frequency was confirmed.

Finally, for testing the heating effect in a realistic arrangement, a spherical sample of 6 mm diameter pressed from magnetite powder of sample III was embedded in the above described KCl/Carrageenan gel and exposed to an alternating magnetic field (amplitude $H_{\text{ext}} = 18$ kA/m, frequency 300 kHz). The surface temperature of the sphere was measured as a function of time with a Cu-Constantan thermocouple attached to the sample. Experimental results are plotted in Fig. 9 and are compared with theoretical curves calculated with $P = 4$ W/cm³ taken from the above discussed experiments and reasonable values for the magnetite sphere ($\lambda_1 = 0.4$ W/mK, $c_1 = 2$ J/gK, $\rho_1 = 2.6$ g/cm³) and the gel (λ_2, ρ_2, c_2 of water). Since the thermocouple was pasted to the surface of the sphere, the radius r was not exactly defined. Therefore,

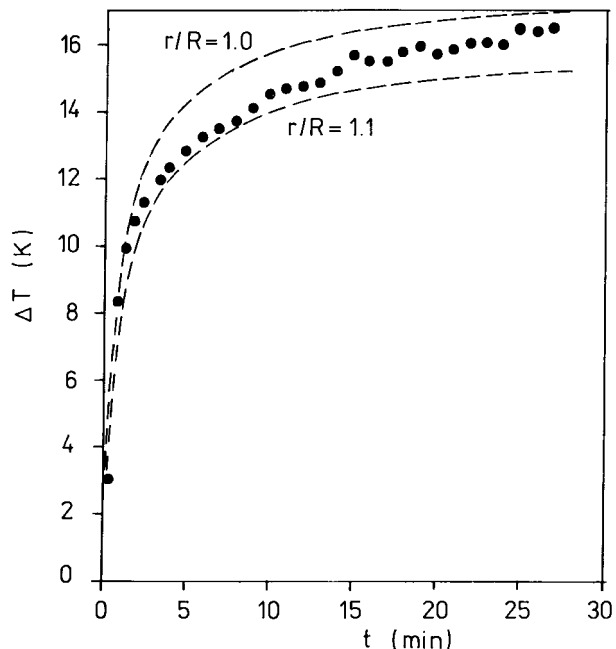


Fig. 9. Measured temperature rise at the surface of a magnetite sphere (6 mm diameter) compared with curves calculated with parameters taken from the experiment or chosen according to reasonable estimations (see text). The two theoretical curves refer to distances of 3.0 and 3.3 mm, respectively, in order to account for a possible small gap between sphere and thermocouple (external magnetic field amplitude 17.6 kA/m, frequency 300 kHz).

two values of r (3 and 3.3 mm) were calculated and plotted in Fig. 9. The main uncertainty of the calculated curves is caused by the evaluation of P for which the external field H_{ext} was transferred to the field H_i acting inside the sphere by

$$H_i = H_{\text{ext}} / (1 + \chi/3) \quad (8)$$

where the susceptibility χ of magnetite of sample type III was measured by means of a hysteresemeter as described in Section III-A. Fig. 9 demonstrates that even with the unfavorable material III, a temperature rise of more than 10 K can be realized for a sphere of 6 mm diameter. However, one has to keep in mind that the equilibrium temperature as expressed by the reduced ordinate in Fig. 7(a) is proportional to the square of the sphere diameter if all other parameters are constant. Accordingly, for our example the rise of surface temperature of a sphere of 1 mm diameter would be less than 1 K. The used model of a spherical heat source of compacted magnetite particles gives an estimation of the heat depletion effects but it is of course a relatively simple approximation. In practice, there will be an inhomogeneous distribution of magnetite particles in the tumor region corresponding to a spatially varying power density. For a quantitative understanding, the magnetite distribution in the tissue which depends on the application method must be known. To attack this problem, heating experiments with liver tissue were performed. In this case microspheres containing magnetite particles were injected as aqueous suspension into pig liver tissue placed in the above described coil. Already after a few minutes of application of rf-power, necrotic effects in the tissue were observed. The results of those in-vitro hyperthermia experiments combined with histological investigations of the thermal cell damaging

have been reported elsewhere [19]. In principle, there are no objections for in-vivo experiments. Especially, there is no risk of toxic effects of unheated magnetite in the present range of applied doses as was already shown by Chan *et al.* [3]. However, one of the most important presupposition for clinical application is the realization of a reliable heating control.

V. CONCLUSIONS

The above reported experimental results combined with the theoretical discussion of various loss mechanisms under different experimental conditions allow one to draw some general conclusions regarding the physical limitations of hyperthermia using fine magnetite particles. Two types of loss mechanisms were found to be of interest for hyperthermia: hysteresis losses and relaxational losses. Both loss types show a nonmonotonous dependence of loss power on particle size i.e., there exist optimum grain sizes which are different for both loss mechanisms. Hysteresis losses increase with decreasing particle size due to increasing remanence and coercivity until relaxation effects appear. There, in a narrow transition region to superparamagnetic behavior, remanence and coercivity decrease abruptly. At the same region considerable Néel losses arise which may be nearly of the same order of magnitude as hysteresis losses. However, these losses are restricted to a very small region of particle sizes. Particle size below the critical size results in rapid decrease of the loss power available for magnetic heating.

For magnetic single domain particles with high uniaxial anisotropy, hysteresis losses are superior to all other losses—provided that the field amplitude is sufficient to ensure the remagnetization of the particle. If there are technical limits for the field amplitude, the coercivity of the magnetic material has to be chosen properly in order to meet this condition. Since coercivity and remanence depend strongly on microstructure, the heating effect may vary appreciably for magnetic particles of different manufacturers. In particular, losses of multidomain particles may be even higher than losses of single domain particles having large uniaxial anisotropy. If in the latter case only a very small fraction of particles of the ensemble are remagnetized, losses may be by orders of magnitude smaller than the theoretical limit given by the anisotropy energy. The above given estimations have shown that at least for small field amplitudes superparamagnetic particles may give power density values being comparable to ferromagnetic ones. However, the influence of size distribution is even more critical in this case and is not appropriately considered in literature until now.

Choosing high power magnetic particles combined with appropriate technical parameters of the external rf-field, very small amounts of magnetic fine particles in the order of tenth of milligrams may easily be used to rise the temperature of biological tissue locally up to cell necrosis. In the stationary state, which may be controlled by the field amplitude and frequency of the external ac field, there is a universal spatial temperature distribution outside of a heated spherical volume which besides by the applied power is determined by the heat

conductivity of the surrounding medium and the radius of the application space. Knowledge of this temperature distribution in dependence on time is a necessary presupposition for a successful elimination of tumors by local magnetic hyperthermia. The achievement of a well-defined magnetite distribution within the tissue is one of the main tasks to be solved on the way to a useful therapy.

ACKNOWLEDGMENT

The authors would like to thank Dr. D. V. Berkov for fruitful discussions. They thank Dipl.-Phys. A. Daum for measurements as well as Dipl.-Phys. R. Bähring and C. Grosser for experimental assistance.

REFERENCES

- [1] R. K. Gilchrist, R. Medal, W. D. Shorey, R. C. Hanselman, J. C. Parrot, and C. B. Taylor, "Selective inductive heating of lymph nodes," *Ann. Surgery*, vol. 146, pp. 596–606, 1957.
- [2] A. A. Luderer, N. F. Borrelli, J. N. Panzarino, G. R. Mansfield, D. M. Hess, J. L. Brown, and E. H. Barnett, "Glass-ceramic-mediated, magnetic-field-induced localized hyperthermia: response of a murine mammary carcinoma," *Radiation Res.*, vol. 94, pp. 190–198, 1983.
- [3] D. C. F. Chan, D. B. Kirpotin, and P. A. Bunn, Jr., "Synthesis and evaluation of colloidal magnetic iron oxides for the site specific radiofrequency-induced hyperthermia of cancer," *J. Magnetism Magn. Mater.*, vol. 122, pp. 374–378, 1993.
- [4] T. Sato, A. Masai, Y. Ota, H. Sato, H. Matuski, T. Yanada, M. Sato, N. Kodama, and S. Minakawa, "The development of anticancer agent releasing microcapsule made of ferromagnetic amorphous flakes for intratissue hyperthermia," *IEEE Trans. Magn.*, vol. 29, pp. 3325–3330, 1993.
- [5] A. Jordan, P. Wust, H. Fähling, W. John, A. Hinz, and R. Felix, "Inductive heating of ferromagnetic particles and magnetic fluids: physical evaluation of their potential for hyperthermia," *Int. J. Hyperthermia*, vol. 9, pp. 51–68, 1993.
- [6] E. Kneller, "Theory of the magnetization curve of small crystals," in *Encyclopedia of Physics*, vol. XVIII/2, Ferromagnetism, H. P. J. Wijn, Ed. New York: Springer-Verlag, 1966, pp. 438–544.
- [7] S. Chikazumi, *Physics of Magnetism*. Philadelphia, PA: Lippincott, 1964.
- [8] F. Heider, D. J. Dunlop, and N. Sugiura, "Magnetic properties of hydrothermally recrystallized magnetite crystals," *Science*, vol. 236, pp. 1287–1290, 1987.
- [9] L. Néel, "Influence of thermal fluctuations on the magnetization of ferromagnetic small particles," *C. R. Acad. Sci.*, vol. 228, pp. 664–668, 1949.
- [10] ———, "Thermoremanent magnetization of fine powders," *Rev. Mod. Phys.*, vol. 25, pp. 293–296, 1953.
- [11] M. I. Shliomis, "Magnetic fluids," *Sov. Phys.—Usp.*, vol. 17, pp. 153–184, 1963.
- [12] R. F. Butler and S. K. Banerjee, "Theoretical single-domain grain size range in magnetite and titanomagnetite," *J. Geophys. Res.*, vol. 80, pp. 4049–4058, 1975.
- [13] H. Pfeiffer, "Relaxation behavior of magnetite particle assemblies due to thermal fluctuations," *Phys. Stat. Sol. (a)*, vol. 120, pp. 233–245, 1990.
- [14] D. V. Berkov, private communication, unpublished.
- [15] W. T. Coffey, P. J. Cregg, and Yu. P. Kalmykov, "On the theory of Debye and Néel relaxation on single domain ferromagnetic particles," *Adv. Chem. Phys.*, vol. LXXXIII, pp. 263–464, 1993.
- [16] L. D. Landau and E. M. Lifshitz, *Electrodynamics of Continuous Media*. London, U.K.: Pergamon, 1960.
- [17] Z. P. Chen and R. B. Roemer, "The effect of large blood vessels on temperature distributions during simulated hyperthermia," *J. Biomechanical Eng.*, vol. 114, pp. 473–481, 1992.
- [18] H. S. Carslaw and J. C. Jaeger, *Conduction of Heat in Solids*. Oxford, U.K.: Clarendon, 1959.
- [19] I. Hilger, W. Andrä, R. Bähring, A. Daum, R. Hergt, and W. A. Kaiser, "Evaluation of temperature increase with different amounts of magnetite in liver tissue samples," *Investigative Radiology*, vol. 32, pp. 705–712, 1997.